

Greatly Enhanced Intermolecular π -Dimer Formation of a Porphyrin Trimer Radical Trications through Multiple π Bonds

Atsuro Takai,^[a] Claude P. Gros,^[b] Jean-Michel Barbe,^{*,[b]} and Shunichi Fukuzumi^{*,[a, c]}

Abstract: A trefoil-like porphyrin trimer linked by triphenylamine (TPA-TPZn₃) was synthesized. A three-electron oxidation of TPA-TPZn₃ forms a radical trication (TPA-TPZn₃³⁺), in which each porphyrin ring undergoes a one-electron oxidation. The radical trication TPA-TPZn₃³⁺ spontaneously dimerizes to afford (TPA-TPZn₃)₂⁶⁺ in CH₂Cl₂. The characteristic charge-resonance band due to the charge delocalization over the π system of (TPA-TPZn₃)₂⁶⁺ was observed in the NIR

region. The initial oxidation potential of TPA-TPZn₃ is negatively shifted relative to that of the corresponding monomer porphyrin, which results from the stabilization of the oxidized state of TPA-TPZn₃ associated with the dimerization. The thermodynamic parameters (i.e., ΔH , ΔS , and ΔG) for

the formation of (TPA-TPZn₃)₂⁶⁺ were determined by measuring Vis/NIR spectra at various temperatures. The formation constant of (TPA-TPZn₃)₂⁶⁺ is significantly larger than that of the radical cation dimer of the corresponding monomer porphyrin (e.g., over 2000-fold at 233 K). The electronic states were investigated using EPR spectroscopic analysis. The greatly enhanced dimerization of TPA-TPZn₃³⁺ results from multiple π -bond formation between the porphyrin radical cations.

Keywords: dimerization • electron transfer • electronic structure • multiple bonds • pi interactions

Introduction

Electronic communication between π -conjugated molecules plays a crucial role in efficient energy transfer and electron transfer not only in biological systems, such as the photosynthetic process,^[1,2] but also in organic electroconductive networks, such as polythiophene and phthalocyanine.^[3] Electron-transfer reactions in these systems are often governed by electronic interactions (e.g., geometry and expansion of π conjugation) and electrostatic interactions (e.g., π - π interactions)^[4] between adjacent chromophores. Even though π -conjugated molecules are similarly charged, a strong electronic interaction which fully compensates the electrostatic repulsion can exist through mediating counterions^[5] and π -bond formation.^[6-8] Formation of a stable π -radical cation

dimer and π -radical anion dimer of aromatic compounds are widely known as a result of π bonding between radical cations and radical anions, respectively.^[7,8]

Such an electronic interaction between aromatic radical ions is expected to manipulate the electron-transfer process.^[5,6a,9] In particular, a significant electronic interaction exists between dimeric bacteriochlorophylls in the photosynthetic reaction center, the so-called special pair, when it undergoes a one-electron oxidation, thereby leading to efficient and unidirectional electron transfer in the natural photosystem.^[9] Thus, much attention has been focused on the electronic interactions between two or more porphyrins in the oxidized state from the point of view of bio-inspired chemistry^[6,10-15] in addition to supramolecular chemistry in the design of highly organized assemblies that consist of porphyrin π systems.^[6b,15,16] In this context, we have reported the effect of electronic interactions in cofacial porphyrin π -dimer radical cations on the dynamics of photoinduced electron transfer.^[6a]

A porphyrin π -radical cation dimer gains larger stabilization energy in the π orbital than a π -dimer radical cation because of the lack of an electron in the antibonding π orbital. Electronic interactions between porphyrin π -radical cations, therefore, lead to distinctly different spectroscopic and structural properties from those in porphyrin π -dimer radical cations.^[6a,11,13a] Recently, we reported the intramolecular electronic interactions between porphyrin radical cations in a multi-porphyrin system.^[6b] However, there has so far been no report on intermolecular electronic interactions of extensive (multiple) π -conjugated macrocycles. If multiple π bonds are formed between multiple porphyrin radical cations, the intermolecular electronic interactions would be sig-

[a] A. Takai, Prof. Dr. S. Fukuzumi
Department of Material and Life Science
Graduate School of Engineering
Osaka University
2-1 Yamada-oka, Suita, Osaka 565-0871 (Japan)
Fax: (+81) 6-6879-7370
E-mail: fukuzumi@chem.eng.osaka-u.ac.jp

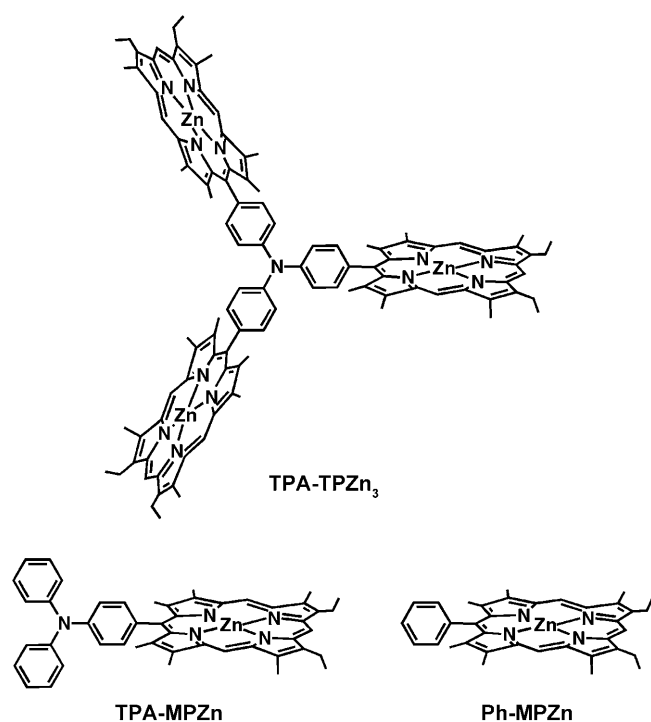
[b] Dr. C. P. Gros, Dr. J.-M. Barbe
ICMUB, UMR CNRS 5260
Université de Bourgogne
9 Avenue Alain Savary, BP 47870, 21078 Dijon Cedex (France)
E-mail: jean-michel.barbe@u-bourgogne.fr

[c] Prof. Dr. S. Fukuzumi
Department of Bioinspired Science
Ewha Womans University
Seoul 120-750 (Korea)

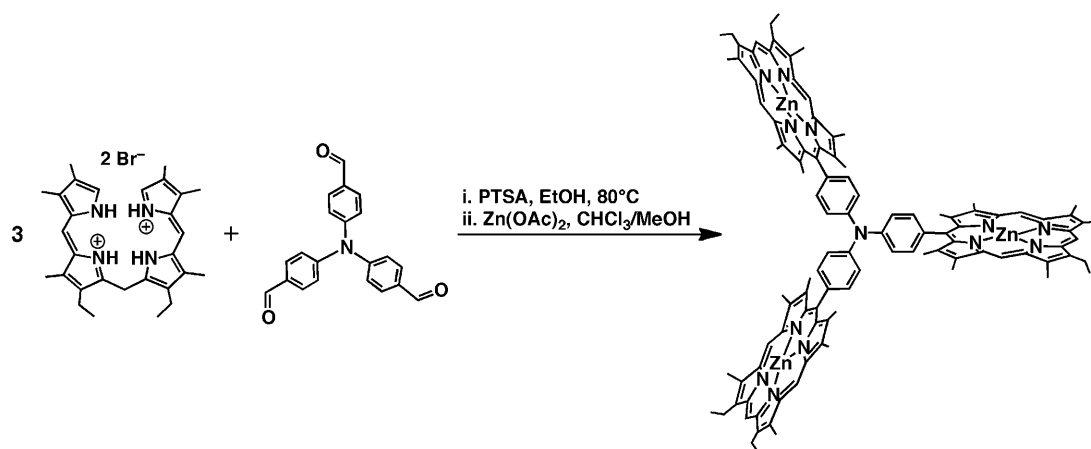
Supporting information for this article is available on the WWW under <http://dx.doi.org/10.1002/chem.201002822>.

nificantly enhanced relative to the case of a monomeric porphyrin radical cation, in contrast to the case of electron (or hole) hopping through weak electronic interactions over multiple electron donors.^[14,17]

We report herein, for the first time, the effects of multiple π bonds on the dimerization equilibria of π -conjugated macrocycle radical cations. We employed a novel porphyrin trimer that consists of a trefoil scaffold TPA-TPZn₃ (Scheme 1). The corresponding monomer porphyrin involving triphenylamine and phenyl groups (TPA-MPZn and Ph-MPZn, respectively) were also investigated for comparison. The TPA moiety is a reasonable linker to enhance the nucleophilicity of porphyrins and to link three porphyrin units independently.^[18]



Scheme 1. Structure of TPA-TPZn₃, TPA-MPZn, and Ph-MPZn.



Scheme 2. Synthesis of TPA-TPZn₃.

Strong π bonding between porphyrin radical cations results in charge delocalization and spin coupling, which can be experimentally recognized by characteristic NIR absorption bands and distinctive changes in EPR spectra.^[7] Thus, the electron-transfer properties of TPA-TPZn₃, TPA-MPZn, and Ph-MPZn were evaluated based on Vis/NIR and EPR spectroscopic analysis and electrochemical measurements. As a result, a remarkably large formation constant of the π -dimer complex of the radical trication TPA-TPZn₃³⁺ was obtained relative to those of the monomer radical cations TPA-MPZn^{•+} and Ph-MPZn^{•+}.

Results and Discussion

Synthesis and characterization: A new type of efficient one-step synthesis of a C_{3v}-symmetrical porphyrin trimer is described herein (Scheme 2). Following reported methodologies,^[19,20] *a,c*-biladiene dibromide was dissolved in ethanol and mixed with tris(aminophenylaldehyde) in the presence of *para*-toluenesulfonic acid (PTSA), followed by metalation with zinc(II) ions. Classical purification of the crude reaction mixture with column chromatography on silica gel with dichloromethane as an eluent gave the tris(porphyrin) tris(zinc) complex (TPA-TPZn₃) in 33% yield. A similar porphyrin preparation was carried out by the condensation of *a,c*-biladiene and 4-(diphenylamino)benzaldehyde to synthesize the corresponding monomer porphyrin TPA-MPZn in 57% yield. The detailed experiments and spectroscopic data of TPA-TPZn₃ and TPA-MPZn are given in the Experimental Section and Supporting Information.

Intermolecular π -bond formation between porphyrin radical cations: Figure 1 shows the UV/Vis spectra of TPA-TPZn₃, TPA-MPZn, and Ph-MPZn. The Soret and Q bands of TPA-TPZn₃ are slightly blue shifted relative to those of TPA-MPZn and Ph-MPZn, contrary to the case of the cofacial porphyrin dimer^[6a,21] and trimer,^[6b] for which red shifts are observed relative to the corresponding monomer porphyrins.

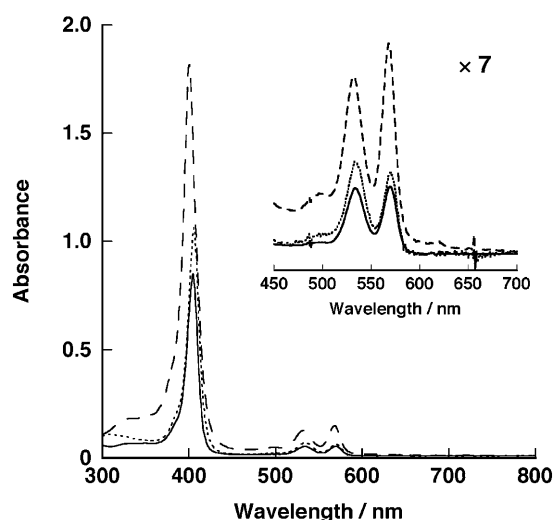


Figure 1. UV/Vis spectra of TPA-TPZn₃ (dashed line), TPA-MPZn (dotted line), and Ph-MPZn (solid line) at 3.0×10^{-6} M in CH₂Cl₂ at 298 K.

The optimized structure of TPA-TPZn₃ obtained by DFT calculations (B3LYP/3-21G) reveals that each porphyrin is geometrically independent and is nearly orthogonal to the TPA moiety (83°; Figure S1 in the Supporting Information). These results indicate that there are little electronic interactions among the porphyrin units of TPA-TPZn₃ in the neutral form.

The Vis/NIR spectral changes upon electron-transfer oxidation of the porphyrin units were recorded to investigate possible electronic interactions between porphyrin moieties in the oxidized state. Figure 2 shows the Vis/NIR titration of TPA-TPZn₃ with the one-electron oxidant [Ru(bpy)₃]³⁺

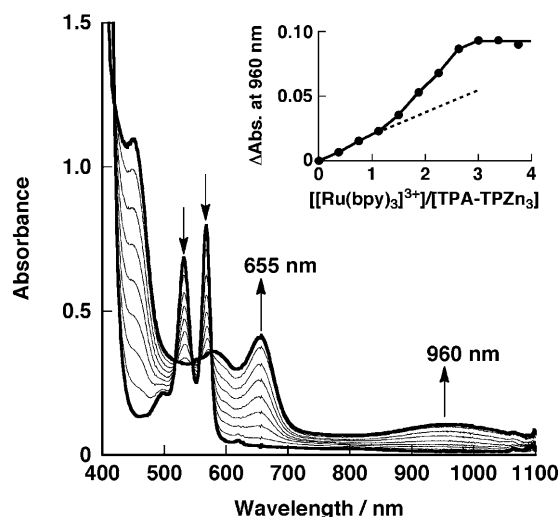
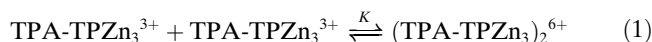


Figure 2. Vis/NIR spectral changes upon the addition of [Ru(bpy)₃]³⁺ ions ($0\text{--}4.3 \times 10^{-5}$ M) to a solution of TPA-TPZn₃ in CH₂Cl₂ (1.4×10^{-5} M) at 298 K. Inset: Plot of ΔA value at $\lambda = 960$ nm versus the concentration ratio of added [Ru(bpy)₃]³⁺/TPA-TPZn₃.

(bpy = 2,2'-bipyridine).^[22] Upon addition of three equivalents of [Ru(bpy)₃]³⁺ ions to a solution of TPA-TPZn₃ in CH₂Cl₂ at 298 K, new absorption bands at $\lambda = 655$ and 960 nm appear. The absorbance at $\lambda = 960$ nm slightly increases until the addition of approximately one equivalent of [Ru(bpy)₃]³⁺ ions followed by a large increase to give the largest value at a ratio of 3:1 for the concentration of [Ru(bpy)₃]³⁺ to the concentration of TPZn₃³⁺, at which point the porphyrin units had undergone a one-electron oxidation (inset, Figure 2). No increase in absorbance is observed by the addition of over three equivalents of [Ru(bpy)₃]³⁺ ions (Figure S2 in the Supporting Information). The absorption band at $\lambda = 655$ nm is typically assigned to the monomer porphyrin radical cation.^[23] This outcome indicates that the initial three-electron oxidation of TPA-TPZn₃ forms TPA-TPZn₃³⁺, in which each porphyrin ring has undergone a one-electron oxidation.

Meanwhile, there are two possibilities to explain the NIR absorption band at $\lambda = 960$ nm: 1) an intervalence charge-transfer (IVCT) band between the porphyrin radical cations through the TPA linker and 2) a charge-resonance band due to the intermolecular π -bond formation between the porphyrin radical cations. To clarify this point, concentration dependence of the Vis/NIR spectrum of TPA-TPZn₃³⁺ were measured. Figure 3a shows the spectral changes of TPA-TPZn₃³⁺ at various concentrations. The ratio of absorbances at $\lambda = 960$ and 655 nm (A_{960}/A_{655}) increases with an increase in the concentration of TPA-TPZn₃³⁺ (inset, Figure 3a). If the NIR absorption was assigned to an IVCT band, the A_{960}/A_{655} values would be the same irrespective of the concentration of TPA-TPZn₃³⁺.^[24] Thus, the NIR absorption is assigned to the charge-resonance band due to the dimerization of TPA-TPZn₃³⁺.^[25] Equation (1) is an equilibrium of the dimerization of TPA-TPZn₃³⁺, in which K is the formation constant of (TPA-TPZn₃)₂⁶⁺, as described below in detail. The radical cation of Ph-MPZn (Ph-MPZn^{•+}) exhibits a small NIR absorption ($\lambda_{\text{max}} = 1020$ nm) under more concentrated conditions relative to the case of TPA-TPZn₃³⁺ at low temperatures (Figure S3 in the Supporting Information). This result indicates that TPA-MPZn^{•+} hardly dimerizes to form a radical cation dimer. When two equivalents of [Ru(bpy)₃]³⁺ ions are added to a solution of TPA-MPZn in CH₂Cl₂, new absorption bands are observed (Figure S4a in the Supporting Information). The absorption bands are in accordance with that observed for pristine TPA in the presence of one equivalent of [Ru(bpy)₃]³⁺ ions (Figure S4b in the Supporting Information).^[24,26] The second oxidation of TPA-MPZn, therefore, occurs at the TPA moiety.



In contrast, the Vis/NIR spectra of TPA-MPZn in the presence of one equivalent of [Ru(bpy)₃]³⁺ ions only shows an absorption at $\lambda_{\text{max}} = 655$ nm due to the monomer porphyrin radical cation and little change in the NIR region (Figure 3b). The A_{960}/A_{655} value is small (ca. 0.05) and constant throughout the change in the concentration of TPA-MPZn^{•+}.

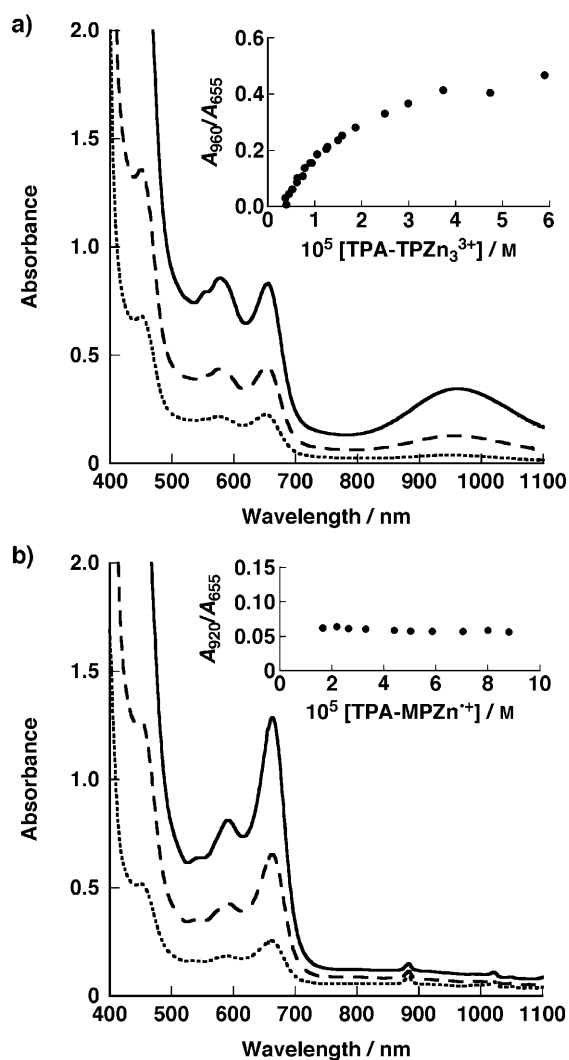


Figure 3. a) Vis/NIR spectral changes of TPA-TPZn₃³⁺ at 3.7 × 10⁻⁵ M (solid line), 1.9 × 10⁻⁵ M (dashed line), and 9.4 × 10⁻⁶ M (dotted line) in CH₂Cl₂ at 298 K. Inset: The ratio of absorbances at λ = 960/655 nm (A₉₆₀/A₆₅₅) versus concentration of TPA-TPZn₃³⁺. b) Vis/NIR spectral changes of TPA-MPZn⁺ at 8.8 × 10⁻⁵ M (solid line), 4.4 × 10⁻⁵ M (dashed line), and 1.7 × 10⁻⁶ M (dotted line) in CH₂Cl₂ at 298 K. Inset: The ratio of absorbance at λ = 920/655 nm (A₉₂₀/A₆₅₅) versus [TPA-MPZn⁺]⁺.

The differences in the electron-transfer oxidation processes of the porphyrin units were also investigated by using cyclic voltammetry (CV) and differential pulse voltammetry (DPV; Figure 4). Ph-MPZn (Figure 4a) exhibits two reversible redox waves, which are typical for the stepwise oxidation processes of the porphyrin rings: Ph-MPZn/Ph-MPZn^{•+} and Ph-MPZn^{•+}/Ph-MPZn²⁺ (0.69 and 0.99 V, respectively). Similarly the first oxidation of TPA-MPZn (Figure 4b) occurs at the porphyrin ring (0.68 V). The second oxidation (0.88 V) is attributed to the oxidation of the TPA moiety, on the basis of the Vis/NIR spectroscopic analysis. Differential pulse voltammograms of the free-base porphyrins Ph-MPH₂ and TPA-MPH₂ also indicate that the TPA moiety is oxidized after the formation of the porphyrin radical cation

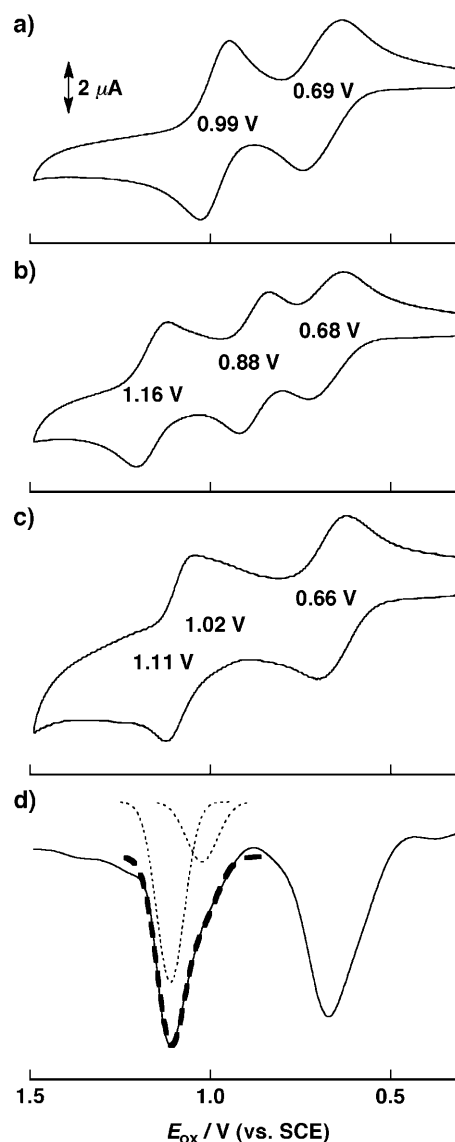


Figure 4. Cyclic voltammograms (100 mV s⁻¹) of a) Ph-MPZn, b) TPA-MPZn, and c) TPA-TPZn₃ (4 × 10⁻⁴ M) in CH₂Cl₂ containing 0.1 M TBAPF₆. d) Differential pulse voltammogram of TPA-TPZn₃ under the same conditions as the cyclic voltammetry. The dashed line is the simulation curve from using two discrete Gaussian-shape oxidation waves (dotted lines).

(Figure S5 in the Supporting Information). The third redox waves of TPA-MPZn (1.16 V) is, thus, assigned to the second oxidation of the porphyrin ring.

The redox behavior of TPA-TPZn₃ is shown in Figure 4c,d. The initial three-electron oxidation process was at 0.66 V, and the second three-electron oxidation process occurred at 1.11 V^[27] with a shoulder at 1.02 V, thus indicating the presence of another redox process. The DPV of TPA-TPZn₃ can be simulated by two Gaussian-shape oxidation waves: two oxidation potentials at 1.02 and 1.11 V were obtained with a ratio of current intensity of 1:3. This outcome indicates that the TPA moiety is oxidized at 1.02 V, whereas the second oxidation of the porphyrin rings in TPA-TPZn₃

takes place at 1.11 V. The positive shifts of the second oxidation of the porphyrin rings in TPA-MPZn and TPA-TPZn₃ with respect to Ph-MPZn result from the electrophilicity of the oxidized TPA moiety. In contrast, the negative shift of the first oxidation potential of TPA-TPZn₃ follows from the stabilization of the oxidized state of TPA-TPZn₃ associated with the dimerization,^[28] although the electrostatic repulsion between porphyrin radical cations induces the destabilization. The electron donation from the TPA to porphyrin moiety may also contribute to the negative shift of the first oxidation potential of TPA-TPZn₃.

Enhanced dimerization of the TPA-TPZn₃ radical cation through multiple π -bond formation: The formation constant K of (TPA-TPZn₃)₂⁶⁺ in Equation (1) was determined from the absorbance change at $\lambda=960$ nm by using Equation (2), in which A_{960} is the absorbance at $\lambda=960$ nm, ε_D is the molar absorption coefficient of (TPA-TPZn₃)₂⁶⁺ at $\lambda=960$ nm, and $[C]$ is the total concentration of TPA-TPZn₃³⁺.

$$(A_{960}/\varepsilon_D)^{1/2} = (K)^{1/2}([C]-2A_{960}/\varepsilon_D) \quad (2)$$

The ε_D value is determined to be $4.6 \times 10^4 \text{ M}^{-1} \text{ cm}^{-1}$ from the temperature-modulated absorption changes at the monomer and dimer band maxima (Figure 5).^[6a,7d] The change in absorbance at $\lambda=960$ nm at various concentrations of TPA-TPZn₃³⁺ at 298 K is shown in Figure 6a. From the linear plot of $(A_{960}/\varepsilon_D)^{1/2}$ versus $[C]-2A_{960}/\varepsilon_D$, the K value is determined to be $1.0 \times 10^4 \text{ M}^{-1}$ at 298 K (inset, Figure 6a). The K values were similarly determined at various temperatures to show a linear correlation between $\ln(K/\text{M}^{-1})$ and T^{-1} (Figure 6b). This van't Hoff plot gives thermodynamic parameters for the formation of (TPA-TPZn₃)₂⁶⁺: $\Delta H = -13.7 \text{ kcal mol}^{-1}$ and $\Delta S = -28.0 \text{ cal K}^{-1} \text{ mol}^{-1}$.

Analogous procedures were repeated to investigate the formation equilibrium of (Ph-MPZn)₂²⁺. Figure S7 a, b in the

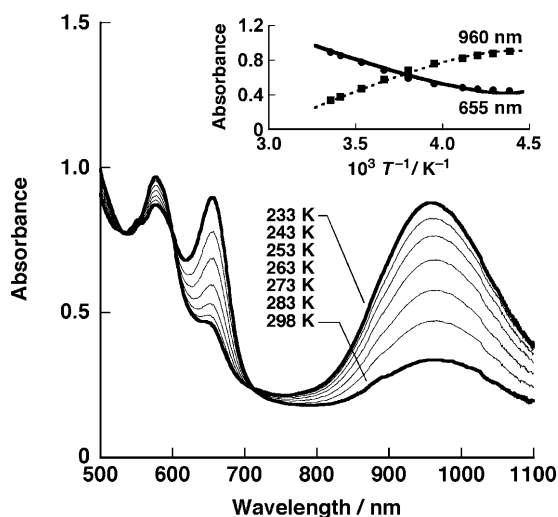


Figure 5. Vis/NIR spectral changes of a solution of TPA-TPZn₃³⁺ in CH₂Cl₂ ($4 \times 10^{-5} \text{ M}$) at various temperatures. Inset: The absorbance changes at $\lambda=655$ and 960 nm.

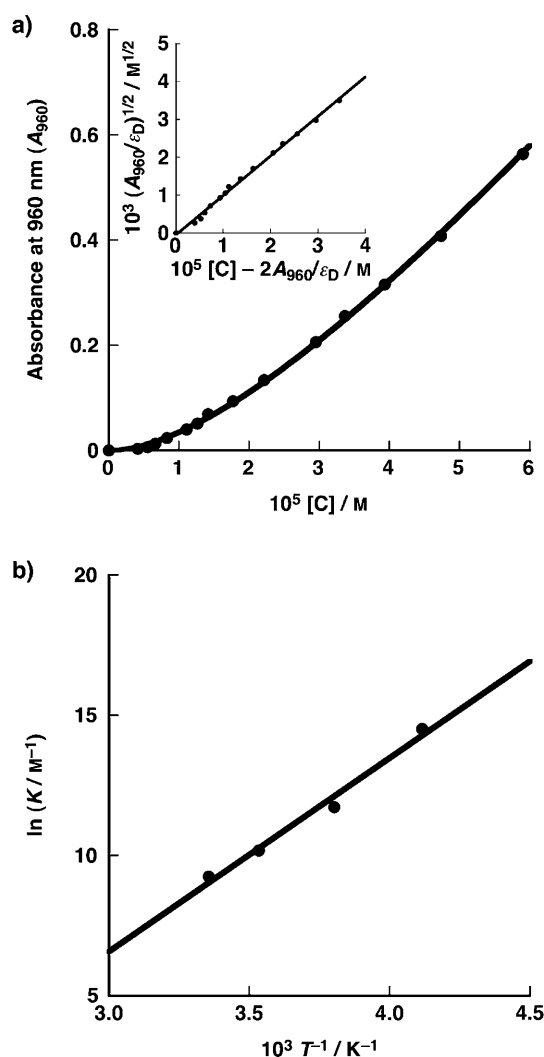


Figure 6. a) The change in absorbance at $\lambda=960$ nm at various concentrations of TPA-TPZn₃³⁺ ($[C]$) at 298 K. Inset: Plot of $(A_{960}/\varepsilon_D)^{1/2}$ versus $([C]-2A_{960}/\varepsilon_D)$. b) van't Hoff plot for the formation constant of (TPA-TPZn₃)₂⁶⁺.

Supporting Information shows the Vis/NIR spectral changes of Ph-MPZn²⁺ at various temperatures and the van't Hoff plot for the formation constant of (Ph-MPZn)₂²⁺, respectively. The formation constants and thermodynamic parameters of (Ph-MPZn)₂²⁺ and of (TPA-TPZn₃)₂⁶⁺ are summarized in Table 1. The formation constant of (TPA-TPZn₃)₂⁶⁺ is much larger than that of (Ph-MPZn)₂²⁺ at any temperature. The formation enthalpy of (TPA-TPZn₃)₂⁶⁺ is significantly more negative than that of (Ph-MPZn)₂²⁺ ($\Delta H = -13.7$ and $-5.9 \text{ kcal mol}^{-1}$, respectively). These results indicate that (TPA-TPZn₃)₂⁶⁺ is stabilized by forming three π bonds at each porphyrin moiety. A nonlinear increase in the absorbance at $\lambda=960$ nm upon the electron-transfer oxidation of TPA-TPZn₃ (Figure 2) indicates that once the first π bond is formed the second and third π -bond formations are significantly enhanced. The structural restriction by multiple π bonding between porphyrin radical cations in (TPA-TPZn₃)₂⁶⁺ leads to a more negative formation entropy than

Table 1. Formation constants (K), thermodynamic parameters (ΔH , ΔS , and ΔG), and absorption maximum (λ_{\max}) of charge-resonance bands for $(\text{TPA-TPZn}_3)_2^{6+}$ and $(\text{Ph-MPZn})_2^{2+}$ in CH_2Cl_2 at various temperatures.

	T [K]	K [M^{-1}]	ΔG [kcal mol^{-1}]	ΔH [kcal mol^{-1}]	ΔS [$\text{cal K}^{-1} \text{mol}^{-1}$]	λ_{\max} [nm]
$(\text{TPA-TPZn}_3)_3^{6+}$	243	2.0×10^6	-6.9			
	263	1.2×10^5	-6.3			
	283	2.6×10^4	-5.8	-13.7	-28.0	960
	298	1.0×10^4	-5.4			
$(\text{Ph-MPZn})_2^{2+}$	233	2.6×10^3	-3.6			
	253	7.7×10^2	-3.4			
	263	5.1×10^2	-3.3	-5.9	-9.9	1020
	273	4.3×10^2	-3.2			
	298	$(1.5 \times 10^2)^{[a]}$	-3.0			

[a] Little increase in the absorbance at $\lambda = 1020$ nm was observed to preclude the precise determination of the K value from Vis/NIR spectroscopy. The value in parenthesis is the K value estimated from the ΔG value at 298 K.

that of $(\text{Ph-MPZn})_2^{2+}$. Nevertheless, the gain in enthalpy that results from strong π -bond formation fully compensates for the loss in entropy to afford a larger stabilization free energy for $(\text{TPA-TPZn}_3)_2^{6+}$ than for $(\text{Ph-MPZn})_2^{2+}$. The difference in the free energy between $(\text{TPA-TPZn}_3)_2^{6+}$ and $(\text{Ph-MPZn})_2^{2+}$ is $\Delta\Delta G = 2.4 \text{ kcal mol}^{-1}$ ($\pm 0.10 \text{ eV}$) at 298 K, in accordance with the value estimated from the difference in the absorption maxima of charge resonance bands $\lambda_{\max} = 60 \text{ nm}$ ($\pm 0.08 \text{ eV}$). To the best of our knowledge, this example is the first that exhibits the synergistic effect of the number of π -conjugated macrocycles on the formation of dimeric radical cations.

The DFT(B3LYP/3-21G basis set) calculation also supports the multiple π -bond formation between porphyrin radical cations in $(\text{TPA-TPZn}_3)_2^{6+}$ (Figure 7a). The mean plane distance between the porphyrin plane and its adjacent counterpart is approximately 3.5 \AA ,^[29] which is close to reported values.^[11a,b,12] The electrostatic potential map for $(\text{TPA-TPZn}_3)_2^{6+}$ together with the observation of NIR absorption bands indicates that positive charges are delocalized over the whole π system (Figure 7b; colored in red), contrary to the case of electron hopping in π -conjugated macrocycles.^[6a,10,14,30]

The spin states in $(\text{TPA-TPZn}_3)_2^{6+}$ were investigated by EPR spectroscopic analysis. Figure 8 shows the temperature dependence of the EPR spectra of TPA-TPZn_3^{3+} in CH_2Cl_2 . The EPR intensities of the samples were quantitatively evaluated using 1,1-diphenyl-2-picrylhydrazyl (DPPH) as an external standard (see the Experimental Section for details). The EPR intensities assigned to TPA-TPZn_3^{3+} changes reversibly and decreases to nearly zero on lowering the temperature. It is estimated from EPR intensity that over 90% of TPA-TPZn_3^{3+} exists as $(\text{TPA-TPZn}_3)_2^{6+}$ at 233 K, which is fairly consistent with the data of the temperature-modulated Vis/NIR spectroscopic measurements (Figure 5). Therefore, the remarkable decrease in the EPR signal intensity can be attributed to the intermolecular spin coupling in the dimer species $(\text{TPA-TPZn}_3)_2^{6+}$. Because of this antiferromagnetic spin coupling, no triplet signal for $(\text{TPA-TPZn}_3)_2^{6+}$ was observed at 77 K, contrary to the case of directly linked porphyrin dimer dications.^[31] The formation

constant K of $(\text{TPA-TPZn}_3)_2^{6+}$ estimated from EPR spectroscopic measurements is larger ($3 \times 10^4 \text{ M}^{-1}$ at 293 K) than that determined from Vis/NIR spectroscopy because the apparent EPR intensity of TPA-TPZn_3^{3+} is slightly less (Figure S8 in the Supporting Information), which leads to an overestimation of the K value.^[32] However, it should be noted that the change in EPR intensity of $(\text{TPA-TPZn}_3)^{n+}$ ($0 \leq n \leq 3$) corresponds well to the increase in ΔA value at $\lambda = 960 \text{ nm}$ due to dimeric species (inset,

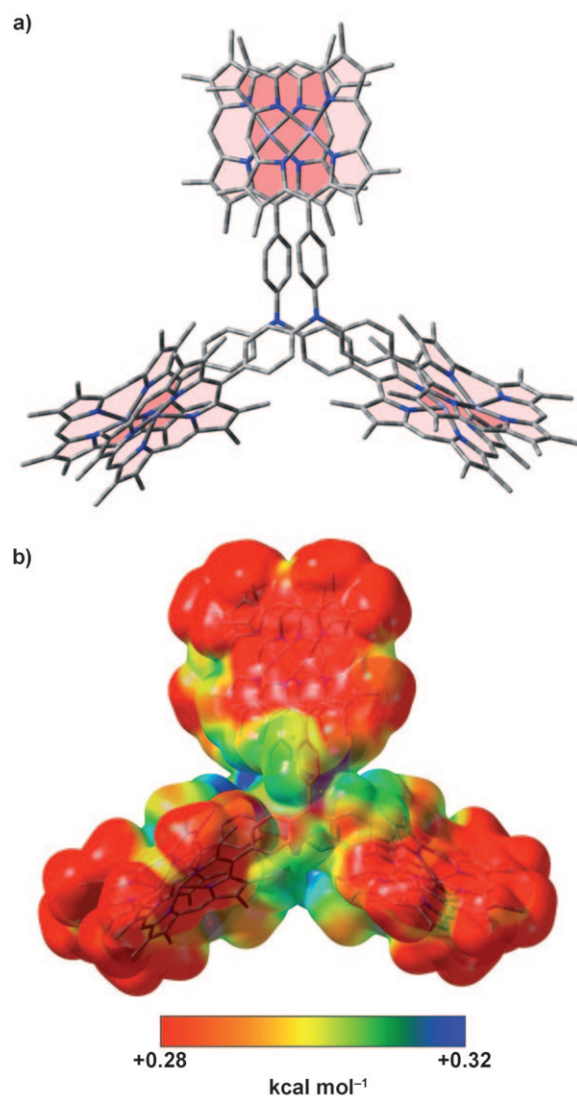


Figure 7. a) Optimized structure and b) electrostatic potential map of $(\text{TPA-TPZn}_3)_2^{6+}$ calculated by DFT at the B3LYP/3-21G level. β -Substituents of TPA-TPZn_3 are replaced by methyl groups for simplicity.

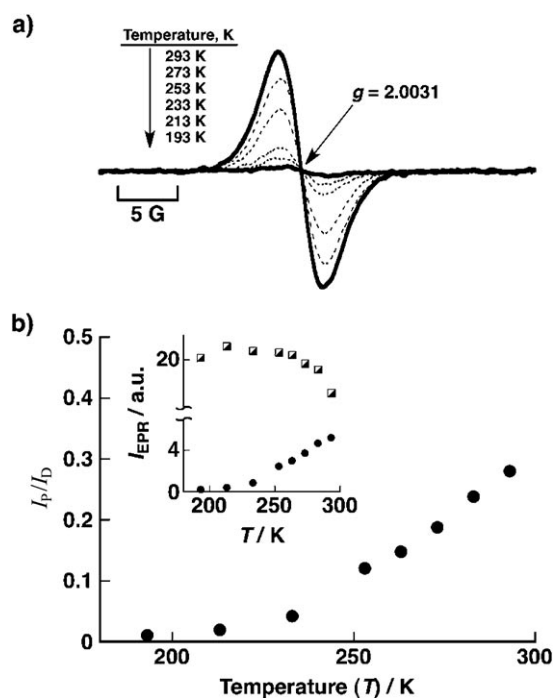


Figure 8. a) EPR spectral changes of a deaerated solution of TPA-TPZn₃³⁺ in CH₂Cl₂ (1.6 × 10⁻⁴ M) in the presence of three equivalents of [Ru(bpy)₃]³⁺ ions at different temperatures. b) Dependence of the ratio of the EPR intensity (I_p/I_D , where I_p and I_D are the EPR intensity of TPA-TPZn₃³⁺ and DPPH, respectively) on the temperature. The EPR intensity was determined by double integration of the corresponding first-derivative EPR spectrum. Inset: Dependence of the EPR intensity (filled circle, I_p ; half-open square, I_D) on the temperature. The concentrations of TPA-TPZn₃³⁺ and DPPH are 1.6 and 4.8 × 10⁻⁴ M in CH₂Cl₂, respectively.

Figure 2). Dependence of EPR intensity on the concentration of TPA-TPZn₃³⁺ (Figure S8c in the Supporting Information) is also in accordance with the UV/Vis titration of TPA-TPZn₃³⁺ at different concentrations (Figure 3a).

Conclusion

The present study has shown that the formation constant of the diamagnetic dimer (TPA-TPZn₃)₂⁶⁺ is remarkably larger than those of radical cation dimers of TPA-MPZn^{•+} and Ph-MPZn^{•+} (e.g., 2000-fold at 233 K). Multiple electronic interactions between porphyrin radical cations in TPA-TPZn₃³⁺ facilitate the formation of a stable diamagnetic dimer cation. Such a synergistic effect can be generalized for a variety of organic π-conjugated macrocycles, which may provide new strategies for the design of organic supramolecular assemblies related to photofunctional and electroconductive materials.

Experimental Section

Chemicals and reagents: Silica gel (Merck; 70–120 mm) was used for column chromatography. Analytical TLC was performed on Merck 60 F254 silica gel (precoated sheets, thickness: 0.2 mm). The reactions were monitored by TLC, UV/Vis spectroscopic, and MALDI TOF mass-spectrometric analysis. Triphenylamine (Tokyo Chemical Industry Co., Ltd.) and 1,1-diphenyl-2-picrylhydrazyl (Wako Pure Chemical Industries, Ltd.) were obtained commercially and used without further purification. The preparation of Ph-MPZn was described elsewhere.^[19a] Tris(2,2'-bipyridyl)ruthenium(III) hexafluorophosphate ([Ru(bpy)₃](PF₆)₃) was prepared from tris(2,2'-bipyridyl)ruthenium(II) chloride hexahydrate by oxidation with PbO₂.^[33] Absolute dichloromethane (Carlo Erba) for synthesis and spectroscopic-grade CH₂Cl₂ and acetonitrile (Nacal Tesque, Inc.) for analysis were obtained commercially and purified prior to use.

Physicochemical and photophysical measurements: ¹H NMR spectra were recorded on a Bruker Avance II 300 (300 MHz) or on a Bruker Avance DRX 500 (500 MHz) spectrometer; chemical shifts are expressed in ppm relative to benzene ($\delta = 7.15$ ppm) or pyridine ($\delta = 7.22$, 7.58, and 8.74 ppm). Mass spectra and accurate mass measurements (HRMS) were obtained on a Bruker Daltonics Ultraflex II spectrometer in the MALDI TOF reflectron mode with dithranol as a matrix or on a Bruker Micro-TOF instrument in ESI mode. Both measurements were made at the Plateforme d'Analyse Chimique et de Synthèse Moléculaire de l'Université de Bourgogne (PACSMUB). UV/Vis/NIR spectra were recorded on a Shimadzu UV-3100PC spectrometer or a Hewlett Packard 8453 diode array spectrophotometer at various temperatures.

Electrochemical measurements: CV and DPV were carried out with a BAS 100W electrochemical analyzer in a deaerated solvent containing 0.10 M tetrabutylammonium hexafluorophosphate (TBAPF₆) as a supporting electrolyte at 298 K. A conventional three-electrode cell was used with a platinum working electrode and a platinum wire as a counterelectrode. The redox potentials were measured with respect to the Ag/AgNO₃ (1.0 × 10⁻² M) reference electrode. The potential values (versus Ag/AgNO₃) are converted into those versus SCE by adding 0.29 V.^[34]

EPR measurements: The EPR spectra were measured at various temperatures with a JEOL X-band spectrometer (JES-RE1XE). The EPR spectra were recorded under nonsaturating microwave-power conditions. The magnitude of the modulation was chosen to optimize the resolution and the signal-to-noise (S/N) ratio of the observed spectra. The g values were calibrated with a Mn²⁺ marker. Solutions of the porphyrins in CH₂Cl₂ were deaerated by purging with argon for 10 min prior to use. The concentrations of the radical species were determined by double integration of the first-derivative EPR signal in reference to that of a known amount of a stable radical, 1,1-diphenyl-2-picrylhydrazyl (DPPH) under the same experimental conditions. Because the radical concentration of DPPH is the same over the entire temperature range, variations in the EPR intensity only depend on the Curie law and instrumental factors such as cavity Q factor. Thus, by comparing the ratio of the EPR intensity of TPZn₃²⁺ (I_p) with that of DPPH (I_D), the radical concentrations of TPZn₃²⁺ can be determined at various temperatures.

Theoretical calculations: DFT calculations were performed on a 32-processor QuantumCube. Geometry optimizations were carried out by using the Becke3LYP functional and 3-21G basis set with the Gaussian 09 program (revision A.02).^[35] The graphics were drawn using the Gauss View software program (version 5.0) developed by Semichem Inc.

2,3,7,8,12,18-Hexamethyl-5-triphenylamine-13,17-diethylporphyrinatozinc (TPA-MPZn): A mixture of 4-(diphenylamino)benzaldehyde (250 mg, 0.915 mmol) and *a,c*-biladiene dihydrobromide (500 mg, 0.829 mmol) was dissolved in hot absolute ethanol (100 mL). PTSA (1.5 g, 8.70 mmol) in ethanol (20 mL) was slowly added over 12 h, and the reaction mixture was stirred and heated to reflux for 48 h. The mixture was cooled to room temperature, and the solution was evaporated under vacuum. The residue was dissolved in dichloromethane (200 mL), neutralized with a saturated solution of NaHCO₃, and washed thoroughly with water (3 × 500 mL). The organic phase was dried over MgSO₄ and filtered, and the solvent was removed in vacuo. The residue was dissolved in chloroform

(35 mL) and methanol (15 mL) and heated to reflux for 90 min in the presence of sodium acetate (89 mg, 1.00 mmol). The metalation reaction was monitored by UV/Vis spectroscopic and MALDI TOF mass-spectrometric analysis. At the end of the reaction, the solvent was removed under reduced pressure and the crude product was dissolved in dichloromethane (50 mL), washed with water (3 × 250 mL), and dried over MgSO₄. The solvent was removed in vacuo and the residue was purified by column chromatography on silica gel (CH₂Cl₂ as the eluent). After evaporation, TPA-MPZn was obtained as a red microcrystalline solid (355 mg, 0.47 mmol, 57%). ¹H NMR (C₆D₆, 298 K): δ = 1.86 (t, *J* = 7.4 Hz, 6H; CH₃), 2.81 (s, 6H; β-CH₃), 3.46 (s, 6H; β-CH₃), 3.51 (s, 6H; β-CH₃), 4.37 (q, *J* = 7.4 Hz, 4H; CH₃-CH₂), 7.11 (dd, 2H; Ph), 7.41 (dd, 4H; Ph), 7.52 (dd, 2H; Ph), 7.64 (dd, 4H; Ph), 7.82 (d, 2H; Ph), 9.80 (s, 1H; H_{meso}), 10.04 ppm (s, 2H; H_{meso}); UV/Vis (CH₂Cl₂): λ_{max} (ε × 10⁻³ M⁻¹ cm⁻¹) = 405.0 (318), 534.0 (17.6), 570.0 nm (15.5); HRMS (MALDI TOF): *m/z*: 755.3002 [M]⁺, 755.2961 calcd for C₄₈H₄₅N₅Zn (see Figure S10 in the Supporting Information).

Triporphyrin tris zinc (TPA-TPZn₃): The triporphyrin tripod (33%, 450 mg, 0.253 mmol) was prepared as described for TPA-MPZn from tris-(aminophenylaldehyde) (250 mg, 0.759 mmol) and *a,c*-biladiene dihydrobromide (1.371 g, 2.27 mmol). ¹H NMR ([D₅]pyridine, 298 K): δ = 1.89 (t, *J* = 8.3 Hz, 18H; CH₃), 3.61 (s, 18H; β-CH₃), 3.65 (s, 18H; β-CH₃), 4.15 (q, *J* = 8.3 Hz, 12H; CH₂), 5.01 (s, 18H; β-CH₃), 6.89 (d, *J* = 8.0 Hz, 6H; Ph), 7.43 (d, *J* = 8.0 Hz, 6H; Ph), 10.46 (s, 3H; H_{meso}), 10.53 ppm (s, 6H; H_{meso}); UV/Vis (CH₂Cl₂): λ_{max} (ε × 10⁻³ M⁻¹ cm⁻¹) = 399.9 (523), 530.0 (54), 570 nm (62); HRMS (MALDI TOF): *m/z*: 1775.6508 [M]⁺, 1775.6485 calcd for C₁₀₈H₁₀₅N₁₅Zn₃ (see Figure S11 in the Supporting Information).

Acknowledgements

This research was supported by Grants-in-Aid (No. 20108010) from the Ministry of Education, Culture, Sports, Science and Technology, Japan and KOSEF/MEST through WCU project (R31-2008-000-10010-0) from Korea. A.T. appreciates a support from the Global COE program "Global Education and Research Center for Bio-Environmental Chemistry" of Osaka University (S.F.) and JSPS fellowship for young scientists. The Centre National de Recherche Scientifique (CNRS, UMR 5260) and "Région Bourgogne" are also acknowledged for funding.

- [1] R. V. Bensasson, E. J. Land, A. L. Moore, R. L. Crouch, G. Dirks, T. A. Moore, D. Gust, *Nature* **1981**, *290*, 329.
- [2] A. A. Pascal, Z. F. Liu, K. Broess, B. van Oort, H. van Amerongen, C. Wang, P. Horton, B. Robert, W. R. Chang, A. Ruban, *Nature* **2005**, *436*, 134.
- [3] a) D. T. McQuade, A. E. Pullen, T. M. Swager, *Chem. Rev.* **2000**, *100*, 2537; b) V. Coropceanu, J. Cornil, D. A. da Silva, Y. Olivier, R. Silbey, J.-L. Bredas, *Chem. Rev.* **2007**, *107*, 926.
- [4] C. A. Hunter, J. K. M. Sanders, *J. Am. Chem. Soc.* **1990**, *112*, 5525.
- [5] a) J. S. Park, E. Karnas, K. Ohkubo, P. Chen, K. M. Kadish, S. Fukuzumi, C. W. Bielawski, T. W. Hudnall, V. M. Lynch, J. L. Sessler, *Science* **2010**, *329*, 1324; b) N. Ise, *Phys. Chem. Chem. Phys.* **2010**, *12*, 10279.
- [6] a) A. Takai, C. P. Gros, J.-M. Barbe, R. Guillard, S. Fukuzumi, *Chem. Eur. J.* **2009**, *15*, 3110; b) A. Takai, M. Chkounda, A. Eggenpiller, C. P. Gros, M. Lachkar, J.-M. Barbe, S. Fukuzumi, *J. Am. Chem. Soc.* **2010**, *132*, 4477.
- [7] a) O. W. Howarth, G. K. Fraenkel, *J. Am. Chem. Soc.* **1966**, *88*, 4514; b) J. K. Kochi, R. Rathore, P. L. Magueres, *J. Org. Chem.* **2000**, *65*, 6826; c) S. Fukuzumi, Y. Endo, H. Imahori, *J. Am. Chem. Soc.* **2002**, *124*, 10974; d) J.-M. Lü, S. V. Rosokha, J. K. Kochi, *J. Am. Chem. Soc.* **2003**, *125*, 12161; e) S. Fukuzumi, H. Kotani, K. Ohkubo, *Phys. Chem. Chem. Phys.* **2008**, *10*, 5159; f) S. Fukuzumi, R. Hanazaki, H. Kotani, K. Ohkubo, *J. Am. Chem. Soc.* **2010**, *132*, 11002.
- [8] a) J. J. Novoa, P. Lafuente, R. E. Del Sesto, J. S. Miller, *Angew. Chem.* **2001**, *113*, 2608; *Angew. Chem. Int. Ed.* **2001**, *40*, 2540; b) R. E. Del Sesto, J. S. Miller, P. Lafuente, J. J. Novoa, *Chem. Eur. J.* **2002**, *8*, 4894; c) J. Yuasa, T. Suenobu, S. Fukuzumi, *J. Am. Chem. Soc.* **2003**, *125*, 12090; d) J. Yuasa, S. Fukuzumi, *J. Am. Chem. Soc.* **2007**, *129*, 12912.
- [9] a) T. P. Treynor, S. S. Andrews, S. G. Boxer, *J. Phys. Chem. B* **2003**, *107*, 11230; b) P. Kanchanawong, M. G. Dahlbom, T. P. Treynor, J. R. Reimers, N. S. Hush, S. G. Boxer, *J. Phys. Chem. B* **2006**, *110*, 18688.
- [10] M. R. Wasielewski, W. A. Svec, B. T. Cope, *J. Am. Chem. Soc.* **1978**, *100*, 1961.
- [11] a) H. S. Song, R. D. Orosz, C. A. Reed, W. R. Scheidt, *Inorg. Chem.* **1990**, *29*, 4274; b) W. R. Scheidt, B. S. Cheng, K. J. Haller, A. Mislankar, A. D. Rae, K. V. Reddy, H. S. Song, R. D. Orosz, C. A. Reed, F. Cukiernik, J. C. Marchon, *J. Am. Chem. Soc.* **1993**, *115*, 1181; c) K. E. Brancato-Buentello, S. J. Kang, W. R. Scheidt, *J. Am. Chem. Soc.* **1997**, *119*, 2839.
- [12] K. M. Barkigia, M. W. Renner, J. Fajer, *J. Phys. Chem. B* **1997**, *101*, 8398.
- [13] a) D. A. Shultz, H. Lee, R. K. Kumar, K. P. Gwaltney, *J. Org. Chem.* **1999**, *64*, 9124; b) S. Fukuzumi, T. Hasobe, K. Ohkubo, M. J. Crossley, P. V. Kamat, H. Imahori, *J. Porphyrins Phthalocyanines* **2004**, *8*, 191; c) M. J. Crossley, P. J. Santic, J. A. Hutchison, K. P. Ghiggino, *Org. Biomol. Chem.* **2005**, *3*, 852; d) G. Pognon, C. Boudon, K. J. Schenk, M. Bonin, B. Bach, J. Weiss, *J. Am. Chem. Soc.* **2006**, *128*, 3488; e) F. D'Souza, R. Chitta, S. Gadde, L. M. Rogers, P. A. Karr, M. E. Zandler, A. S. Sandanayaka, Y. Araki, O. Ito, *Chem. Eur. J.* **2007**, *13*, 916; f) F. D'Souza, E. Maligaspe, K. Ohkubo, M. E. Zandler, N. K. Subbaiyan, S. Fukuzumi, *J. Am. Chem. Soc.* **2009**, *131*, 8787.
- [14] T. M. Wilson, T. Hori, M. C. Yoo, N. Aratani, A. Osuka, D. Kim, M. R. Wasielewski, *J. Am. Chem. Soc.* **2010**, *132*, 1383.
- [15] A. Takai, C. P. Gros, J.-M. Barbe, S. Fukuzumi, *Phys. Chem. Chem. Phys.* **2010**, *12*, 12160.
- [16] a) M. J. Ahrens, R. F. Kelley, Z. E. X. Dance, M. R. Wasielewski, *Phys. Chem. Chem. Phys.* **2007**, *9*, 1469; b) A. de La Escosura, M. V. Martinez-Diaz, D. M. Guldi, T. Torres, *J. Am. Chem. Soc.* **2006**, *128*, 4112; c) A. I. Oliva, B. Ventura, F. Würthner, A. Camara-Campos, C. A. Hunter, P. Ballester, L. Flamigni, *Dalton Trans.* **2009**, 4023.
- [17] S. V. Rosokha, I. S. Neretin, D. Sun, J. K. Kochi, *J. Am. Chem. Soc.* **2006**, *128*, 9394.
- [18] a) F. D'Souza, S. Gadde, D. M. S. Islam, C. A. Wijesinghe, A. L. Schumacher, M. E. Zandler, Y. Araki, O. Ito, *J. Phys. Chem. A* **2007**, *111*, 8552; b) N. K. Subbaiyan, L. Obraztsov, C. A. Wijesinghe, K. Tran, W. Kutner, F. D'Souza, *J. Phys. Chem. C* **2009**, *113*, 8982.
- [19] a) K. M. Kadish, N. Guo, E. Van Caemelbecke, A. Froio, R. Paolesse, D. Monti, P. Tagliatesta, T. Boschi, L. Prodi, F. Bolletta, N. Zaccaroni, *Inorg. Chem.* **1998**, *37*, 2358; b) D. Bellows, S. M. Aly, C. P. Gros, M. E. Ojaimi, J.-M. Barbe, R. Guillard, P. D. Harvey, *Inorg. Chem.* **2009**, *48*, 7613.
- [20] a) B. Franck, G. Krautstrunk, *Liebigs Ann. Chem.* **1993**, 1069; b) S. Kawabata, I. Yamazaki, Y. Nishimura, *Bull. Chem. Soc. Jpn.* **1997**, *70*, 1125.
- [21] a) H. L. Anderson, *Inorg. Chem.* **1994**, *33*, 972; b) A. Satake, Y. Kobuke, *Org. Biomol. Chem.* **2007**, *5*, 1679; c) Z. J. Chen, A. Lohr, C. R. Saha-Moller, F. Würthner, *Chem. Soc. Rev.* **2009**, *38*, 564.
- [22] Other one-electron oxidants, such as tris(4-bromophenyl)ammonium hexachloroantimonate, are also available.
- [23] J. H. Fuhrhop, P. Wasser, D. Riesner, D. Mauzerall, *J. Am. Chem. Soc.* **1972**, *94*, 7996.
- [24] C. Lambert, G. Noll, *J. Am. Chem. Soc.* **1999**, *121*, 8434.
- [25] It is difficult to detect the dimeric species by using either MALDI TOF or ESI mass spectrometry because they may easily decompose into the monomeric species in the gas phase.
- [26] a) E. T. Seo, R. F. Nelson, J. M. Fritsch, L. S. Marcoux, D. W. Leedy, R. N. Adams, *J. Am. Chem. Soc.* **1966**, *88*, 3498; b) K. Sreenath, C. V. Suneesh, V. K. Kumar, K. R. Gopidas, *J. Org. Chem.* **2008**, *73*, 3245.

- [27] The current intensities at 0.66 and 1.11 V are threefold larger than that of ferrocene (Fc/Fc⁺ at 0.49 V versus SCE) under the same conditions, thus confirming that both the first and second oxidation processes of TPA-TPZn₃ are three-electron processes (see Figure S6 in the Supporting Information for CV and DPV analysis).
- [28] Note that the NIR absorption due to (TPA-TPZn₃)₂⁶⁺ is observed, even in the presence of the supporting electrolyte TBAPF₆; hence, the first oxidation potential of TPA-TPZn₃ is strongly associated with the dimerization equilibrium under the present conditions.
- [29] Because porphyrin planes are not strictly flat nor parallel to each other, the plane distance exhibits distribution from 3.2 to 3.7 Å.
- [30] a) C. R. Newman, C. D. Frisbie, D. A. da Silva, J. L. Bredas, P. C. Ewbank, K. R. Mann, *Chem. Mater.* **2004**, *16*, 4436; b) M. J. Tauber, R. F. Kelley, J. M. Giaimo, B. Rytchinski, M. R. Wasielewski, *J. Am. Chem. Soc.* **2006**, *128*, 1782.
- [31] H. Segawa, Y. Senshu, J. Nakazaki, K. Susumu, *J. Am. Chem. Soc.* **2004**, *126*, 1354.
- [32] The diamagnetic character of (TPA-TPZn₃)₂⁶⁺ was also indicated in the ¹H NMR spectrum at low temperature, which exhibits only the signals in the diamagnetic region (Figure S9 in the Supporting Information).
- [33] R. E. Desimone, R. S. Drago, *J. Am. Chem. Soc.* **1970**, *92*, 2343.
- [34] C. K. Mann, K. K. Barnes, *Electrochemical Reactions in Nonaqueous Systems*, Marcel Dekker, New York, **1970**.
- [35] Gaussian 09, Revision A.02, M. J. Frisch, G. W. Trucks, H. B. Schlegel, G. E. Scuseria, M. A. Robb, J. R. Cheeseman, G. Scalmani, V. Barone, B. Mennucci, G. A. Petersson, H. Nakatsuji, M. Caricato, X. Li, H. P. Hratchian, A. F. Izmaylov, J. Bloino, G. Zheng, J. L. Sonnenberg, M. Hada, M. Ehara, K. Toyota, R. Fukuda, J. Hasegawa, M. Ishida, T. Nakajima, Y. Honda, O. Kitao, H. Nakai, T. Vreven, J. A. Montgomery, Jr., J. E. Peralta, F. Ogliaro, M. Bearpark, J. J. Heyd, E. Brothers, K. N. Kudin, V. N. Staroverov, R. Kobayashi, J. Normand, K. Raghavachari, A. Rendell, J. C. Burant, S. S. Iyengar, J. Tomasi, M. Cossi, N. Rega, J. M. Millam, M. Klene, J. E. Knox, J. B. Cross, V. Bakken, C. Adamo, J. Jaramillo, R. Gomperts, R. E. Stratmann, O. Yazyev, A. J. Austin, R. Cammi, C. Pomelli, J. W. Ochterski, R. L. Martin, K. Morokuma, V. G. Zakrzewski, G. A. Voth, P. Salvador, J. J. Dannenberg, S. Dapprich, A. D. Daniels, Ö. Farkas, J. B. Foresman, J. V. Ortiz, J. Cioslowski, D. J. Fox, Gaussian, Inc., Wallingford CT, **2009**.

Received: October 1, 2010
Published online: February 15, 2011